Applied Surface Science 464 (2019) 43–52

Contents lists available at ScienceDirect

Applied Surface Science

journal homepage: www.elsevier.com/locate/apsusc

Full Length Article

Efficient Z-scheme visible-light-driven photocatalytic bacterial inactivation by hierarchical MoS_2-encapsulated hydrothermal carbonation carbon core-shell nanospheres

Tianqi Wang[a], Mingzhe Sun[b], Hongli Sun[a], Jin Shang[b,*], Po Keung Wong[a,*]

[a] School of Life Sciences, The Chinese University of Hong Kong, Shatin, NT, Hong Kong, China
[b] School of Energy and Environment, City University of Hong Kong, Tat Chee Avenue, Kowloon, Hong Kong, China

ARTICLE INFO

Keywords:
MoS_2
Carbon
Z-scheme
Inactivation
Visible light

ABSTRACT

A MoS_2-encapsulated hydrothermal carbonation carbon (HTCC@MoS_2) heterojunction was constructed via a one-pot route. The HTCC@MoS_2 nanospheres could efficiently inactivate 7-log bacterial cells within 50 min. Notably, as a metal-free material, pure HTCC nanostructures fabricated in this work also showed desirable photocatalytic activity. The continuously produced reactive species, especially $^{\cdot}O_2$ radicals, caused significant damage of bacterial cell membrane. The unique Z-scheme mode remarkably promoted the electron transfer and charge separation in the HTCC@MoS_2 composite. This work not only developed a novel strategy for the direct conversion of carbohydrates to metal-free and photocatalytically active HTCC semiconductor, but also provided a promising HTCC@MoS_2 heterojunction for cost-effective water disinfection.

1. Introduction

Every year, numerous people are sickened by waterborne diseases raised from biohazards such as bacteria and viruses in unsafe drinking water [1]. Driven by the public health and environmental concerns, the development of low-cost and robust methods for water disinfection is of great significance. Photocatalysis has been demonstrated to be a "green" and effective disinfection method. Molybdenum disulfide (MoS_2) materials were generally employed as visible-light-driven (VLD) photocatalysts [2–4]. Recent significant advances have focused on designing and fabricating of MoS_2/carbon heterostructures with enhanced photocatalytic performance. For instance, MoS_2/(g-)C_3N_4, MoS_2/graphene (oxide), and MoS_2/graphic carbon composites have been prepared for efficient photocatalytic H_2 production or dye degradation [5–11]. Nevertheless, their wide applications are still limited by the expensive carbon materials [12]. Therefore, it is important to discover a low-cost carbon substitute for the fabrication of carbon-based photocatalysts.

Our recent work reported an ultrathin hydrothermal carbonation carbon (HTCC) coating which was easily derived from glucose [13]. Hu et al. even proposed a strategy to obtain HTCC from agricultural wastes [14]. Hence, the cost of HTCC is significantly lower than that of graphene or C_3N_4. Moreover, other HTCC-contained photocatalysts such as iodine-doped HTCC and CdS/HTCC have been readily prepared and applied for disinfection or dye degradation [14,15]. Unfortunately, the HTCC alone shows extremely low photocatalytic activity due to the serious recombination of photo-generated electron-hole pairs [13,14], thereby it is generally used as a carbon shell to facilitate the electron transfer. Hence, it is of great significance to have an in-depth study on the basis of the following concerns: (1) fabricating HTCC with enhanced photocatalytic activity; and (2) understanding the interaction between the HTCC core and the shell material in a hybrid photocatalytic system.

Herein, we developed the HTCC@MoS_2 composite as an efficient VLD photocatalyst. The nano-sized HTCC also showed noticeable photocatalytic performance. The synergetic effect, band structures, and photocatalytic activities of HTCC and MoS_2 were studied in detail, followed by the investigation of the photocatalytic inactivation mechanisms.

2. Results and discussion

2.1. Material characterization

The XRD spectrum (Fig. 1) collected for the pure HTCC sample confirmed its amorphous structure, because no diffraction was observed. As expected, the HTCC@MoS_2 composite and pure MoS_2 showed almost the same XRD profiles, with two major characteristic peaks located at around 33.0° and 58.3°, which were ascribed to the

* Corresponding authors.
E-mail addresses: jinshang@cityu.edu.hk (J. Shang), pkwong@cuhk.edu.hk (P.K. Wong).

https://doi.org/10.1016/j.apsusc.2018.09.060
Received 9 August 2018; Received in revised form 5 September 2018; Accepted 7 September 2018
Available online 08 September 2018
0169-4332/

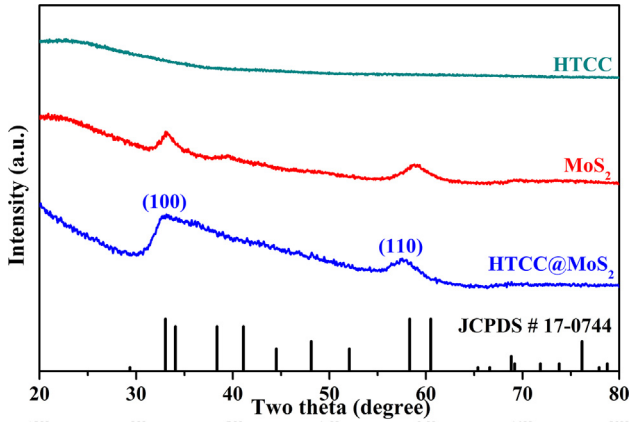

Fig. 1. XRD patterns of HTCC, MoS_2, and HTCC@MoS_2.

(1 0 1) and (1 1 0) planes of hexagonal MoS_2 nanosheets (JCPDS card No. 17-0744), respectively. This result was in good agreement with that of previously reported MoS_2 nanosheets, in which two major peaks at very similar locations were observed [16–18]. As displayed in Fig. 2, the pure HTCC was composed of numerous nanospheres, with the average particle size of ~45 nm, value much smaller than that of previously reported HTCC (e.g. 2–4 μm) [14]. As shown in Fig. 2b, the MoS_2 microspheres with an average diameter of 1 μm were assembled by MoS_2 nanosheets. The HTCC@MoS_2 composite exhibited a uniform spherical morphology with the particle size of ~100 nm (Fig. 2c and Fig. 3a). The TEM images of HTCC@MoS_2 clearly displayed a core-shell structure, and the MoS_2 nanosheets were closely loaded on the HTCC cores (Fig. 3). The thickness of MoS_2 shell and the diameter of HTCC core were estimated to be 8.5 and 83 nm, respectively. As shown in Fig. 3d, the lattice fringe on the shell material was detected to be 0.27 nm, corresponding to the (1 0 1) crystal facet of MoS_2. The elemental mappings were employed to reveal the distributions of Mo, S, and C elements in the HTCC@MoS_2 nanospheres. As shown in Fig. 3e–g, Mo and S elements were uniformly distributed in the MoS_2 shell, while C element was only observed in the HTCC core, which was consistent with the TEM results.

To understand the components and chemical states of the products, XPS and FT-IR measurements were performed. As shown in Fig. 4a and b, intensive signals appeared at 232.4, 229.1, 163.4, and 162.1eV were accordingly assigned to Mo $3d_{3/2}$, Mo $3d_{5/2}$, S $2p_{1/2}$, and S $2p_{3/2}$ peaks [19,20], suggesting the dominant existences of Mo^{4+} and S^{2-} [21,22]. As shown in Fig. 4c and d, the HTCC@MoS_2 nanospheres and HTCC demonstrated very similar C 1s and O1s spectra, revealing that the HTCC component was preserved in HTCC@MoS_2. The XPS results suggested that there was no noticeable change in the chemical states and the major bonds of the HTCC@MoS_2 nanospheres compared with those of pure MoS_2 and HTCC materials. The FT-IR spectra (Fig. S1) confirmed the major carbon component of polyfuran in HTCC and HTCC@MoS_2. For instance, the bands appeared at 1190, 1015, 872, and 625 cm^{-1} were assigned to the C–H modes of polyfuran [13,23,24]. The presence of open furan rings was evidenced by the band at 1703 cm^{-1}, which was in good agreement with previous studies [14,25].

The N_2 adsorption-desorption isotherms of HTCC, MoS_2, and HTCC@MoS_2 were in good agreement with the type III isotherm (Fig. 5a), indicating the nonporous or macroporous structures [26]. As shown in Fig. 5b, the pore sizes of HTCC, MoS_2, and HTCC@MoS_2 were mainly distributed at 92, 55, and 53 nm, respectively, indicating the dominant presence of macro-pores (> 50 nm). Based on the SEM and TEM results, the macro-pores were raised from the non-rigid aggregates of catalyst particles. As shown in Table 1, the HTCC@MoS_2 composite exhibited the largest BET surface area of 25.38 m^2/g. The larger surface area of HTCC@MoS_2 may provide more active sites and benefit the light harvesting.

The mass ratios of the HTCC to the MoS_2 in the HTCC@MoS_2 composites synthesized using different amounts of $Na_2MoO_4{\cdot}2H_2O$ and thiourea were estimated by TG analysis (Fig. S2). The rapid decline occurred at 230–250 °C was caused by the decomposition of HTCC. The mass loss at 250–450 °C was due to the oxidation of MoS_2 to MoO_3 together with the decomposition of residual HTCC [13]. In addition, no more mass loss was observed after 450 °C, suggesting that the remaining product after the TG measurement was pure MoO_3. From the final weight fractions of MoO_3, the mass proportions of MoS_2 were calculated to be 26.9%, 42.9%, and 33.1% for the HTCC@MoS_2-1, HTCC@MoS_2-2, and HTCC@MoS_2 samples, respectively (Table S1).

2.2. Photocatalytic bacterial inactivation performance

As shown in Fig. 6, the HTCC@MoS_2 photocatalyst with the HTCC/MoS_2 mass ratio of 66.9%: 33.1% exhibited the highest VLD photocatalytic efficiency. Thus, this sample with optimized HTCC/MoS_2 mass ratio was selected as the model photocatalyst in the following studies. The bare MoS_2 catalyst could only inactivate 2.4-log bacterial cells within 50 min. By contrast, the *E. coli* K-12 cells were efficiently inactivated when employing the HTCC@MoS_2 nanospheres as the photocatalyst, with a 7-log reduction of bacterial population within 50 min. Considering the photocatalytic efficiency, the HTCC@MoS_2 photocatalyst is among the highest level for VLD photocatalytic inactivation [1,13,27–29]. Moreover, the inactivation kinetics demonstrated a typical "shoulder + loglinear" trend, which was a common observation in photocatalytic bacterial inactivation [30,31]. It is interesting to point out that the pure HTCC, as a metal-free material, exhibited an apparent photocatalytic inactivation ability. A nearly linear decrease in the bacterial density was observed throughout the reaction and about

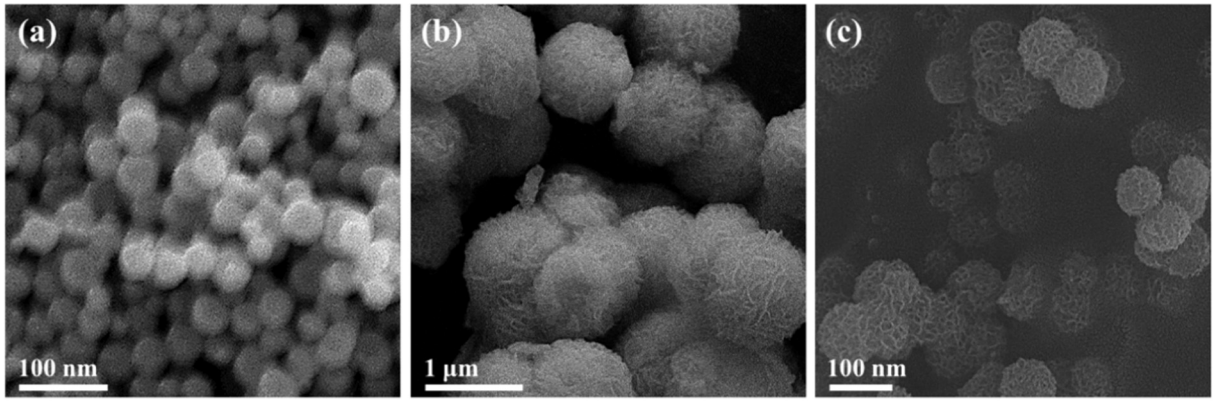

Fig. 2. SEM images of (a) HTCC, (b) MoS_2, and (c) HTCC@MoS_2.